Gold(I)–Thiolate Coordination Polymers as Multifunctional Materials: The Case of Au(I)– p -Fluorothiophenolate

Shefali Vaidya, Saly Hawila, Fan Zeyu, Tuhin Khan, Alexandra Fateeva, François Toche, Rodica Chiriac, Anne Bonhommé, Gilles Ledoux, Sébastien Lebègue, et al.

Gold(I)-thiolate coordination polymers as multifunctional materials, the case of the Au(I)-*para*-fluorothiophenolate

Shefali Vaidya#,[a,b] Saly Hawila#,[a] Zeyu Fan,[c] Tuhin Khan,[d] Alexandra Fateeva,[e] François Toche,[e] Rodica Chiriac,[e] Anne Bonhommé,[a] Gilles Ledoux,[f] Sébastien Lebègue,[g] Jeongmin Park,[h] Won June Kim,[h] Juejing Liu,[i] Xiaofeng Guo,[i] Adel Mesbah,[a] Satoshi Horike,[j,k] and Aude Demessence*[a]

# Equal contribution

[a] Université Claude Bernard Lyon 1, CNRS, IRCELYON – UMR 5256, Villeurbanne 69100, France.

[b] Institute of Experimental and Applied Physics, Czech Technical University in Prague, Prague 110 00, Czech Republic.

[c] Department of Synthetic Chemistry and Biological Chemistry, Graduate School of Engineering, Kyoto University, Katsura, Nishikyo-ku, Kyoto 615-8510, Japan.

[d] Institute of Macromolecular Chemistry, Czech Academy of Sciences, Prague 162 00, Czech Republic

[e] Université Claude Bernard Lyon 1, CNRS, LMI - UMR 5615, Villeurbanne 69622, France.

[f] Université Claude Bernard Lyon 1, CNRS, ILM - UMR 5306, Villeurbanne 69622, France.

[g] Université de Lorraine, CNRS, LPCT - UMR 7019, Vandœuvre-lès-Nancy 54506, France.

[h] Changwon National University, Department of Biology and Chemistry, Gyeongsangnam-do 51140, South Korea.

[i] Department of Chemistry, Washington State University, Pullman, WA 99164, USA.

[j] Department of Chemistry, Graduate School of Science, Kyoto University, Kitashirakawa-Oiwakecho, Sakyo-ku, Kyoto 606-8502, Japan.

[k] Department of Materials Science and Engineering, School of Molecular Science and Engineering, Vidyasirimedhi Institute of Science and Technology, Rayong 21210, Thailand.

KEYWORDS Gold-thiolate, photoluminescence, phase change, coordination polymer glass, composite material

ABSTRACT: Gold-sulphur interaction has a vital importance in nanotechnologies and material chemistry to design functional nanoparticles, self-assembled monolayers or molecular complexes. In this paper, the mixture of only two basic precursors: the chloroauric acid, $HAu(III)Cl_4$, and a thiol molecule, the *para*-fluorothiophenol (*p*-HSPhF) are used for the synthesis of gold(I)-thiolate coordination polymers. Under different conditions of synthesis and external stimuli five different functional materials with different states of $[Au(I)(p\text{-}SPhF)]_n$ can be afforded. These gold-thiolate compounds are (i) red emissive, flexible and crystalline fibers, (ii) composite materials made of these red emissive fibers and gold nanoparticles, (iii) amorphous phase, (iv) transparent glass and (v) amorphous-to-crystalline phase change material associated to a ON/OFF switch of the luminescence. The different functionalities of these materials highlight the great versatility of the gold(I) thiolate coordination polymers with easy synthesis and diverse shaping that may find great potentials as sustainable phosphors, smart textiles, sensors and phase change memories.

Introduction

Gold's strong affinity towards sulphur is a primordial bond found in different domains of coordination chemistry, nanoscience and nanotechnology to form molecular species, stabilized/functionalized gold nanoparticles (AuNPs) or self-assembled monolayers (SAMs).[1-3] These gold-sulphur-based materials have a wide range of applications in the fields of electronics, catalysis, therapeutic agent delivery, and sensing to name a few.[3-7] The nature of the interaction between gold, which may exist in an oxidation state of +III, +I or 0, and the thiol (–SH) or thiolate (–S(-I)) groups in nanomaterials remains a topic of ongoing discussion.[8-9] Gold(I)-thiolate-based coordination polymers (CPs) or oligomers, $[Au(SR)]_n$, are compounds that can be obtained

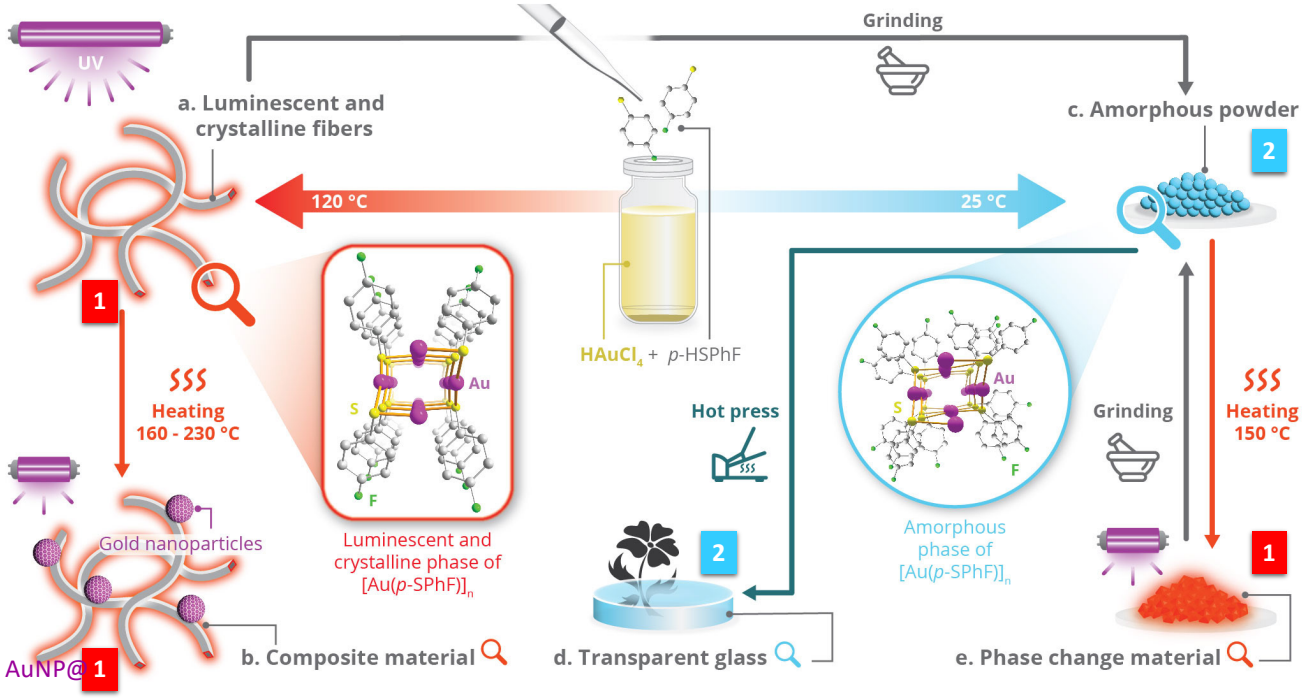

Scheme 1. Schematic representation of the different states of [Au(*p*-SPhF)]$_n$ CP, **1** for crystalline and **2** for amorphous, and the formation processes, as: a. luminescent and crystalline fibers, b. composite material made of fibers and AuNPs, c. amorphous powder, d. transparent glass and e. phase change material.

easily from the oxydo-reduction synthesis between HAu(III)Cl$_4$ and a thiol molecule, HSR.[10-13] This reaction is commonly used as the first step in the synthesis of thiolate-based AuNPs or clusters, prior to the addition of a reducing agent.[14-16] Thus, gold(I)-thiolate compounds are of tremendous importance to understand and control the formation of AuNPs and in some extend the fabrication of SAMs. Therefore, interests in [Au(SR)]$_n$ as nanomaterials and crystalline CPs have gained considerable attention in recent years.[17-18] Structure resolution of some gold(I)-thiolate CPs shows that they adopt a 1D or 2D structure with common Au(I)–S–Au(I) chains, that form double-interpenetrated helices or are parallel, respectively.[12, 17, 19] In addition, Au(I) is a d^{10} metal that exhibits strong photoluminescent properties and can exhibit aurophillic interactions.[20-21] Thus, gold(I)-thiolate CPs can display wide photoemission properties in the solid state and at room temperature (RT) with quantum yields up to 70 %. The energy emissions vary from the yellow region of the visible spectrum to the near-infrared region with possible multiple emission bands for ratiometric thermometry.[12-13, 19, 22]

The softness of these gold-thiolate CPs allows shaping and has been a fruitful strategy to get: flexible (nano)fibers,[23-24] transparent glasses[25] and phase change materials of pure [Au(SR)]$_n$ CPs.[19] Thus, red-emissive and flexible fibers of the crystalline [Au(SPh)]$_n$ CP have been reported. Its 1D structure with double-interpenetrated helices of Au(I)–S–Au(I) chains allows flexibility in the fibers.[23] The controlled decomposition by heating these gold-thiophenolate fibers resulted in the formation of around 70 nm AuNPs on their surface. This composite material can be dispersed in a solution and detect small quantities of *para*-mercaptobenzoic acid thanks to the Surface Enhanced Raman Spectroscopy (SERS) effect of the AuNPs.[23] Gold-thiolate CPs can also be obtained as amorphous phases by using mild synthetic conditions.[25] For the amorphous phases of [Au(SR)]$_n$ (R = Ph, MePh and EtPh) CPs, the pair distribution analyses (PDF) showed that the 1D bonding network of gold-thiolate remains, but the disorder induces the absence of aurophilic interaction and so non-luminescent compounds. Moreover, the mechanical pressing of these amorphous powders allows the direct formation of transparent glasses.[25] Finally, the other distinct feature of these gold thiolate CPs is their ability to exhibit reversible amorphous-to-crystalline phase change in the solid state and by heating-grinding stimuli. Indeed, the crystallization from the amorphous phase can be observed by differential scanning calorimetry (DSC) for [Au(SPh)]$_n$[12] at 204 °C and for [Au(SEtPh)]$_n$ at 140 °C and a crystal-to-crystal phase change is also observed at 190 °C.[19] In addition, the crystallization, from the non-luminescent amorphous phase, induces the formation of red-emissive crystalline phases. Such new and sustainable phase-change materials can provide a good alternative to the toxic inorganic chalcogenide phase-change materials for phase-change memory.[26]

Thus, Au(I)-thiolate CPs are sustainable and versatile materials that can open the doors to various applications. To display their multifunctionality altogether, we report here the study of a new CP, gold(I)-*para*-fluorothiophenolate [Au(*p*-SPhF)]$_n$, and show its ability to form (a.) luminescent and crystalline fibers, (b.) composite materials with AuNPs for molecule detection, (c.) amorphous phase, (d.) transparent glasses and (e.) phase change materials (Scheme 1).

Experimental section

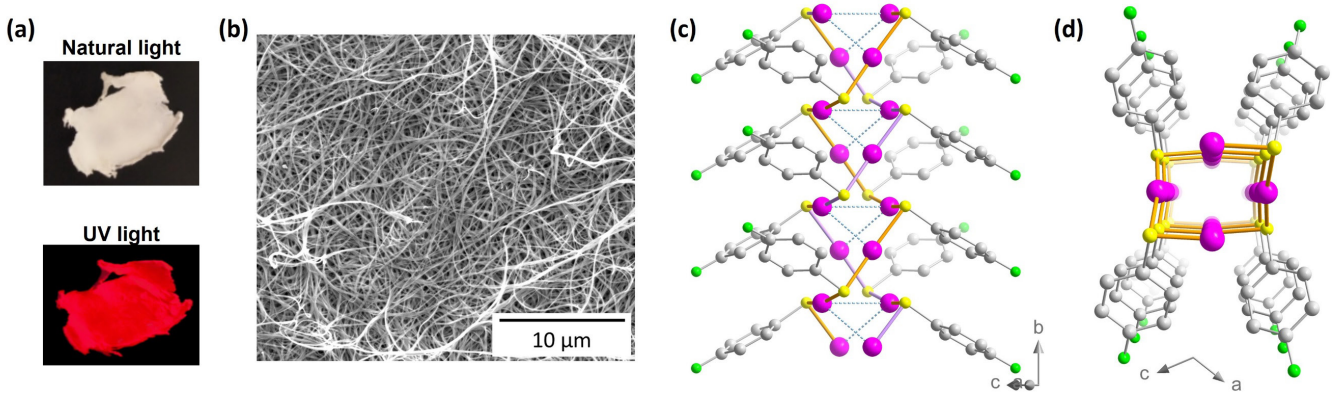

Figure 1. Luminescent and crystalline fibers of [Au(*p*-SPhF)]$_n$ CP. (a) Photographs of the textile-like [Au(*p*-SPhF)]$_n$ (**1**) under natural and UV lights, (b) SEM image of the fibers of **1**. Crystal structure of **1**: (c) view of the two [AuS]$_n$ interpenetrated helices (orange and purple), light blue dashed lines represent the aurophilic interactions and (d) central projection along *b* axis. Pink, Au; yellow, S; light green, F; grey, C. Hydrogen atoms are omitted in c and d for clarity.

Tetrachloroauric acid trihydrate ($HAuCl_4 \cdot 3H_2O$, ≥ 49 % Au basis) was purchased from Alfa Aesar. 4-Fluorothiophenol (98 %) was purchased from Sigma Aldrich. Methanol and ethanol were purchased from VWR Chemicals. All reagents and solvents were used as received.

Synthesis of [Au(*p*-SPhF)]$_n$ fibers (1)

To a solution of $HAuCl_4 \cdot 3H_2O$ (50 mg, 0.127 mmol, 1 eq.) in ethanol (10 mL), *para*-fluorothiophenol (542 µL, 50.89 mmol, 40 eq.) was added. The reaction was allowed to proceed for 18 h at 120 °C in a 20 mL sealed glass vial. A white fibrous precipitate was obtained and washed three times with 50 mL of EtOH. Yield: 73 % (30 mg).

Synthesis of the amorphous [Au(*p*-SPhF)]$_n$ (2)

To the methanolic solution (10 mL) of $HAuCl_4 \cdot 3H_2O$ (50 mg, 0.127 mmol, 1 eq.), *para*-fluorothiophenol (81 µl, 0.763 mmol, 6 eq) was added and the reaction was let to proceed for 1 h at RT in a 20 mL sealed vial. The white precipitate obtained after filtration was washed three times with 20 mL of ethanol. The powder was collected by centrifugation at 10000 rpm. The product was dried in air. Yield: 78 % (32 mg).

Calcination of fibers

The fibers were calcined at a rate of 6 °C.min^{-1} in the temperature range of 160–250 °C. The fibers were kept on a glass plate and pressed on it to make a plain surface for homogenous heating.

Fabrication of the glass of [Au(*p*-SPhF)]$_n$, coordination polymer glass (CPG)

By mechanical pressing: 50 mg of the gently grounded powder of **2** was deposited between highly polished stainless disks of 13 mm diameter and inserted in a Specac™ Atlas™ Evacuable Pellet Die, usually used for KBr pellet production for FTIR analysis samples. For the formation of the coordination polymer glass (CPG) monolith, a pressure of 0.098 MPa (10 tons) was applied for a period of 60 s.

By hot pressing: 20 mg of **2** was deposited between highly polished stainless disks of 5 mm diameter, and inserted in a Pellet die manufactured by S.T. Japan Inc. The opaque pellet formed by the application of 10 MPa for 15 s was sandwiched between metal supports and transferred to the hot press. The hot press was maintained at a temperature of 90 °C. For the first 30 min the pellet was preheated under vacuum and next 30 mins under a pressure of 0.06 MPa (6 kN).

Phase-change experiments

Crystalline-to-amorphous phase change: 20 mg of the crystalline [Au(*p*-SPhF)]$_n$ CP was hand-grounded in an agate mortar pestle for 30 mins in an ambient atmosphere. After grinding the sample becomes amorphous and non-luminescent.

Amorphous-to-crystalline phase change: 20 mg of the amorphous [Au(*p*-SPhF)]$_n$ CP placed in a crucible was heated at 150 °C (with a ramp of 2 °C.min^{-1}) for 1 min under ambient atmosphere. After heating the sample becomes crystalline and red emissive.

Instrumentation details for the various measurements are provided in the ESI.

Result and discussion

a. Luminescent and crystalline fibers of [Au(*p*-SPhF)]$_n$ CP (scheme 1a)

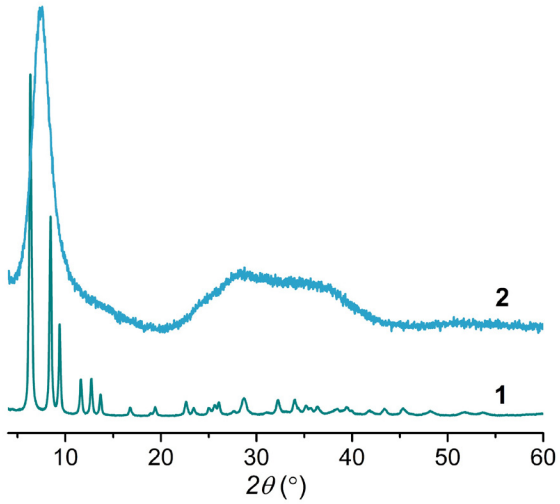

Figure 2. PXRD patterns of the as-synthesized crystalline (**1**) and amorphous (**2**) phases of [Au(*p*-SPhF)]$_n$.

Synthesis and characterizations. The mixture of $HAuCl_4 \cdot 3H_2O$ with an excess of *para*-fluorothiophenol in ethanol at 120 °C for 18 h leads to the formation of a fibrous material: $[Au(I)(p\text{-}SPhF)]_n$ (**1**) (figure 1a). The powder x-ray diffraction (PXRD) pattern shows that it is highly crystalline, with the first reflections at 6.48°, 8.56°, 9.34°, 11.68°, 12.72° and 13.76° in 2θ values (figure 2). The thermogravimetric analysis (TGA) of **1** corresponds to a 1:1 ligand:metal ratio, with the final bulk gold residue of 61.3 % (calculated 60.8 %), confirming the formulae as $[Au(I)(p\text{-}SPhF)]_n$ (figure S1). This TGA experiment carried out in air, shows also that **1** is stable up to 200 °C. Scanning electron microscopy (SEM) images show curved and long fibers of a few micrometers length and a diameter of around 90 ± 26 nm can be observed (figures 1b and S2).

The crystal structure of **1** is solved with high-resolution PXRD data from Soleil synchrotron (figure S3). Compound **1** crystallizes in the monoclinic space group *C2/c* with cell parameters a = 31.6123(18) Å, b = 4.4464(3) Å, c = 21.3106(9) Å and β = 118.766(2) ° (figures 1c and d and table S1). The structure of $[Au(p\text{-}SPhF)]_n$ is similar to $[Au(SPh)]_n$, $[Au(SEtPh)]_n$ and $[Au(o\text{-}SPhCO_2H/Me)]_n$ CPs with a 1D double-interpenetrated helices structure.[12, 19, 27-28] In one helix, the Au cations are coordinated to two sulphur atoms in a quasi-linear fashion, with S–Au–S angles being 161.8 ° and 173.1 ° (table S2). The sulphur atoms bridge two Au cations in a μ_2 coordination mode with angles of 91.4 ° and 104.6 ° (table S2). Aurophilic interactions are present between the two helices, with Au(I)–Au(I) distances of 3.33 and 3.40 Å.[29-31] The Au(I)–S distances are between 2.22 and 2.43 Å. The F atoms being electronegative, a F···H bond network is formed with the neighboring hydrogens of the phenyl rings (figure S4 and table S3).[12, 32]

The infra-red spectrum of **1** shows the absence of the peak corresponding to –SH stretching frequency around 2600-2550 cm^{-1}, which confirms the full deprotonation of the thiol group and the formation of Au(I)-thiolate bonds (figure S5). DFT simulations have been carried out to calculate the IR spectrum of **1** and assign the vibrational bands (figure S6 and Table S4). The calculated FT-IR spectrum of **1** reproduces well the experimental one. As it was reported for the 2D silver-thiolate analog, $[Ag(p\text{-}SPhF)]_n$, **1** displays a similar spectrum with a symmetric vibration ν_s(C=C) observed at 1586 cm^{-1} and calculated at 1580 cm^{-1}.[33] The antisymmetric vibrations ν_{as}(C=C) is observed and calculated at 1392 and 1389 cm^{-1}. Compared to the silver thiolate CP, the vibrational bands of **1** are shifted to the lower energies.

Photoluminescence. As shown on figure 1a, the white fibers of **1** are red-emissive under UV radiation at RT. Absorption spectrum, recorded in the solid state at RT, displays a band centered at 270 nm, that can be attributed to the ligand-centered (LC) π→π* transition of the phenyl ring of the thiolate ligand (figure 3a).[12] The experimental optical band gap is 3.3 eV vs 3.8 eV when calculated with the HSE functional, which neglects electron-hole interactions and hence predict a slightly larger band gap. The excitation curve is quite similar to the absorption, except that two maxima at 265 and 305 nm are present. When **1** is excited at 270 nm, an intense emission band is centred at 720 nm

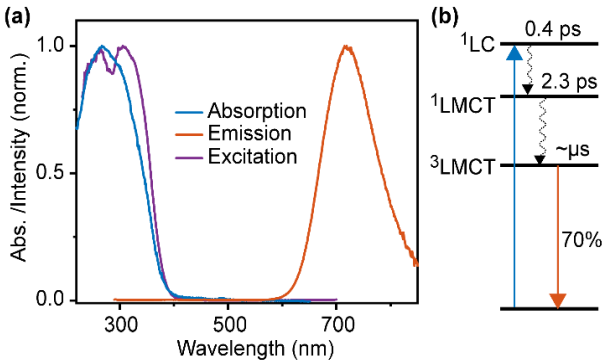

Figure 3. (a) Steady state absorption (blue), excitation monitored at 720 nm) (purple)and emission (excited at 270 nm) (red) spectra of **1** carried out at RT and in solid state. (b) Scheme of the excited states associated with **1**.

(figure 3a). The large Stokes shift of 23100 cm^{-1} is consistent with a phosphorescent process. The quantum efficiency (QY) of emission at RT is found to be around 70 %. The photoemission has been measured from -180 to 110 °C with λ_{ex} = 340 nm (figure S7). This experiment shows that **1** reaches its maximum intensity of emission from -60 °C and below. Increasing the temperature from -60 °C up to 110 °C exhibit a gradual decrease of the emission intensity to almost null, due to the dominance of the non-radiative recombination at high temperatures (Figure S7).[34] Still, a measurable luminescence (~ 3 % QY) of **1** is observed till 110 °C. Gold thiophenolate, $[Au(SPh)]_n$, which has a similar 1D structure to **1**, with slightly longer aurophilic interactions of 3.33, 3.37 and 3.60 Å, exhibits an emission maximum centred at 684 nm and a QY around 5 % at RT.[12] Its emission process has been attributed to LMMCT (Ligand-to-Metal-Metal Charge Transfer). Thus, the presence of the

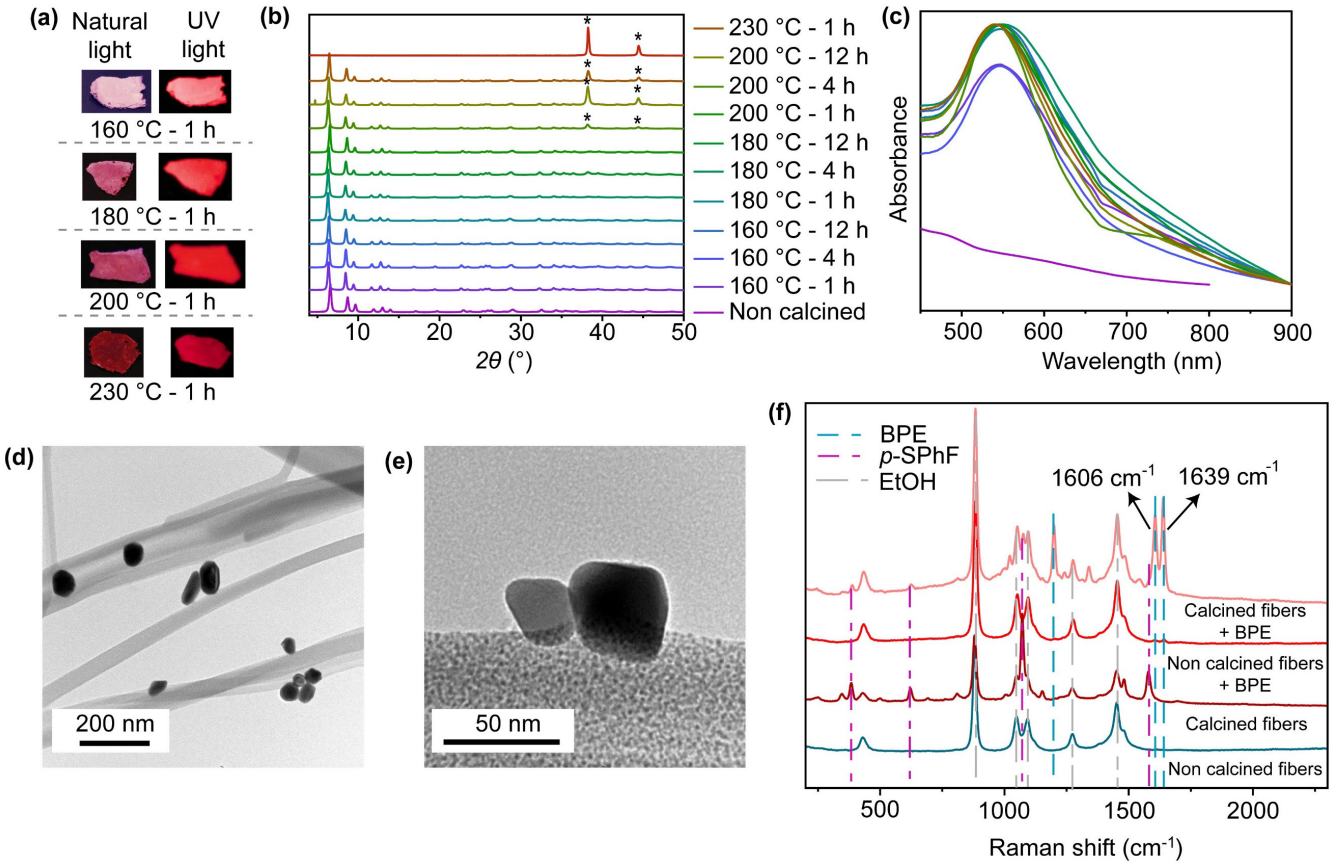

Figure 4. AuNPs@[Au(*p*-SPhF)]$_n$ composite material. (a) Photographs under natural (left) and UV (right) lights of [Au(*p*-SPhF)]$_n$ fibers (**1**) calcined under air at 160 °C, 180 °C, 200 °C and 230 °C for 1 h. (b) PXRD patterns and (c) solid-state UV-Vis spectra of the fibers calcined at different temperatures and times. (d) and (e) TEM images of the fibers calcined at 230 °C for 1 h. (f) Comparison of the Raman spectra of non-calcined and calcined [Au(*p*-SPhF)]$_n$ fibers with and without BPE molecule.

fluorine, as an electron-withdrawing group, and shorter aurophilic interactions (two times 3.33 and 3.40 Å), induce a red shift of the emission and a much higher QY.[35-38]

At room temperature, microsecond excited state decay with an average lifetime of 5.6 µs is measured (Figure S8). This long lifetime with the large Stokes supports that the emission is phosphorescent involving a triplet ligand to metal charge transfer (^{3}LMCT) state.[19,39] The emission peak position and shape remain unchanged upon variation of the excitation wavelength (figure S9). Additionally, the excitation spectra (monitored at the emission peak) match closely with the absorption peak confirming that there is only one emissive state which is also directly coupled to the absorbing ligand-centered state. Furthermore, no variation in the emission peak position is noticed in the temperature range of -180 °C to 110 °C (Figure S7). Lack of emission in the UV-visible region (300-650 nm) from any of the various gold thiolate CPs that have been measured (sample not presented here), indicates that the intersystem crossing from the singlet to the triplet state is ultrafast in nature.[40] Thus, to have a close look into its formation process(es), femtosecond pump probe spectroscopy is taken. A broad excited state absorption spanning the entire probe range of 500-900 nm is observed (Figure S10a) and possibly associated with the luminescent state (^{3}LMCT). Kinetic trace monitored at the peak shows an ultrafast rise of the excited state absorption signal (Figure S10b) confirming that the triplet state is formed through an excited state process (Figure 3b). Two ultrafast components of 0.4 ps and 2.3 ps were extracted. Based on the expected excited state evolution (^{1}LC → ^{1}LMCT → ^{3}LMCT),[39] we assign the 0.4 ps component to the ^{1}LC state and the 2.3 ps to the ^{1}LMCT state (Figure 3b). Such picosecond singlet lifetime has been reported for transition metal complexes, including Au(I).[40-43] Since there is a π-σ* (bond breaking) state in close proximity to the π-π* (absorbing) state of the thiophenol moiety,[44] this could affect the ^{1}LC → ^{1}LMCT transition of CPs and their subsequent luminescence yield. This may be the reason why little to no luminescence is observed in its amorphous phase (**2**).

b. Composite material AuNPs@[Au(*p*-SPhF)]$_n$ (scheme 1b)

The formation of bifunctional AuNPs@[Au(*p*-SPhF)]$_n$ composites, made of gold nanoparticles and luminescent [Au(*p*-SPhF)]$_n$ CPs, were obtained by calcination of the fibers of **1** under air in the temperature range of 160 °C to 250 °C for various time (1, 4 and 12 h) to induce the partial decomposition of the CPs (figure 4). After calcination, the white samples turn pink, purple, red or brown when the temperature/time increases and more importantly, keep their fibrous aspect and their red emission under UV light at RT (figures 4a and S11). The apparition of these colors is due

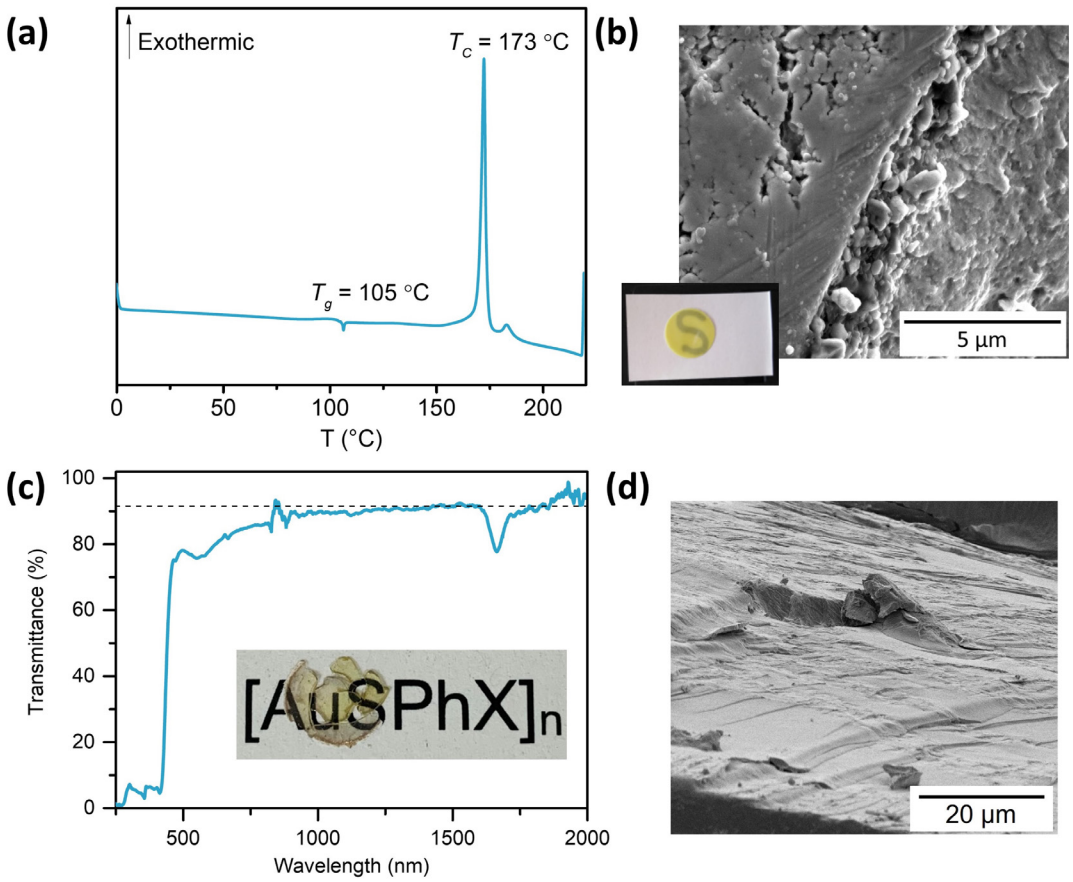

Figure 5. Amorphous phase and glass of [Au(*p*-SPhF)]$_n$. CP. (a) DSC of **2** under air at 10 °C.min^{-1}. (b) SEM images of **2g$_1$** with its photograph, (c) % transmittance of the glass prepared by hot-press, **2g$_2$**, with its photograph (gray dotted line: baseline) and (d) its SEM image.

to the presence of gold nanoparticles and their surface plasmon resonance (SPR).[45] The PXRD patterns of the calcined samples show that **1** remained crystalline till 230 °C (figure 4b). When the fibers are calcined at 250 °C for 1 h, the CP completely decomposes, the organic part is transformed into gases and only bulk gold remains on the PXRD. From the PXRD patterns, the presence of bulk gold can be seen from calcination at 200 °C. So, UV-visible spectroscopy of the different calcined samples is carried out to confirm the presence of AuNPs (figure 4c). For samples calcined at 160 °C to 230 °C, an absorption band around 550 nm can be seen corresponding to the SPR band of AuNPs of less than 100 nm.[46-47] With increasing the temperature, the band is broader and red-shifted, meaning that the AuNPs get bigger and/or gold nanorods are present, which is confirmed by the longitudinal SPR peak at 750 nm and on some TEM images (figures 4c and S11-S13). All the calcined samples exhibit an emission band centered at 720 nm, as it was reported for **1**, except the one calcined at 250 °C that contains only bulk gold (figure S14-S15). The SEM images of the samples calcined at 200 °C for 1 and 12 h, and at 230 °C for 1h are collected (figure S16). These SEM images show that the AuNPs are homogeneously dispersed on the surface of the [Au(*p*-SPhF)]$_n$ fibers. To get better resolution and to measure the size of the AuNPs, TEM images are collected (figures 4d and e and S11 – S13). The AuNP size measured from the samples calcined at 180 °C – 12 h, 200 °C – 1 h, 200 °C – 12 h and 230 °C – 1 h are 31 ± 8 nm, 24 ± 7 nm, 47 ± 17 nm and 49 ± 18 nm, respectively. This is in good accordance with the UV-vis experiments and points out that the increase of the temperature and time induce a slight increase of the AuNPs diameter and also their polydispersity.

AuNPs with SPR are well known for their SERS effect, which can be used for the detection of molecules.[23, 48-51] As demonstrated earlier, AuNPs supported on gold-thiolate fibers can be efficient reusable materials for the detection of para-mercaptobenzoic acid.[23, 52] In this study, AuNPs@[Au(*p*-SPhF)]$_n$ composite fibers were used with the 1,2-bis(4-pyridyl)ethylene (BPE) as the probing molecule.[53-55] The fibers calcinated at 230 °C – 1h were chosen as the source of AuNPs of 49 ± 18 nm. For carrying out the studies, fibers (non-calcined and calcined) were dispersed in ethanol. The Raman spectrum of the non-calcined fibers alone shows the peaks corresponding to ethanol itself whereas the calcined fibers alone showed the bands corresponding to ethanol and *p*-fluorothiophenolate (383, 621, 1071, 1152, 1481, 1579 cm^{-1}) (figure 4f). This observation means that the presence of the AuNPs in the calcined sample can detect the thiolate ligand. Next, the Raman spectrum of non-calcined fibers with BPE (2.5 x 10^{-3} M) was collected. Again, the peaks correspond to ethanol and the BPE molecule cannot be detected, because there are no AuNPs on the non-calcined fibers. The spectrum of the calcined fibers along with

BPE (2.5 x 10^{-3} M) showed bands analogous to the BPE molecule (1606 and 1639 cm^{-1}), in addition to the 4-fluorothiophenolate and ethanol. The appearance of these two new peaks confirms that the composite AuNPs@[Au(*p*-SPhF)]$_n$ material shows SERS effect and can detect the BPE molecule.

c. Amorphous phase of [Au(*p*-SPhF)]$_n$ CP (scheme 1c)

The reaction of $HAuCl_4 \cdot 3H_2O$ with *para*-fluorothiophenol in EtOH at RT for 1 h results in the formation of the amorphous phase of [Au(*p*-SPhF)]$_n$ (**2**). Indeed, the PXRD of **2** reveals a broad peak between 4-11° with a maximum at 7.4 ° and a large massif in the 20-40 ° region in 2θ values, pointing out its low crystallinity (figure 2). The PXRD feature of **2** is similar to the gold-thiolate amorphous compounds previously reported, which means that the -S-Au-S- chains are maintained.[25] The TGA and the chemical analysis of **2** correspond to the same formula of **1** as [Au(I)(*p*-SPhF)]$_n$ (figure S1). The SEM of **2** shows that this amorphous phase is composed of aggregated nanoparticles of less than 100 nm (figure S17). The white-off powder is not emissive at RT and exhibits weak emission centered at 710 nm at -150 °C (figure S18). The Differential Scanning Calorimetry (DSC) of **2** under air reveals a glass transition (T_g) and crystallization peak (T_c) at 105 °C and 173 °C, respectively, before the decomposition starting at 185 °C (figure 5a). When DSC is carried out under N_2 the T_g is shifted to 95 °C and T_c to 180 °C (figure S19). The crystallization behavior will be discussed in detail in part e.

d. Transparent glass of [Au(*p*-SPhF)]$_n$ CP (scheme 1d)

Because **2** holds a T_g, the amorphous [Au(*p*-SPhF)]$_n$ CP has the ability to form glass (figure 5). Thus, coordination polymer glass can be either formed with a mechanical press at RT or with a hot press. The initial method involves applying a mechanical pressure of 0.098 MPa to 50 mg of powder of **2** at room temperature. This results in an opaque glass, $\mathbf{2g_1}$, with a diameter of 13 mm and a thickness of 143 µm. (figure 5b and S20).[25] The PXRD of the glass matches the amorphous phase (figure S21). The SEM images of the glass $\mathbf{2g_1}$ show a plain surface with some dense area and also some pores (figures 5b and S20). The presence of these grain boundaries implies light scattering and opacity of the glass. To improve the transparency of the CPG, hot-press method has been used. Hot press of **2** at 90 °C in vacuum and then under 0.06 MPa at 90 °C for a total of 1h provided a coordination polymer glass [Au(*p*-SPhF)]$_n$ ($\mathbf{2g_2}$) with high transparency up to 90 % in the infrared region (figure 5c). The transmittance decreases steadily to 75 % in the visible region before suddenly dropping to zero at around 430 nm. The SEM image of $\mathbf{2g_2}$, without pores is in good accordance with its transparency (figure 5d). This study points out that the use of hot-press results in the formation of CPG with better transparency.

e. Reversible amorphous-crystalline phase-change in [Au(*p*-SPhF)]$_n$ CP (scheme 1e)

As it has been mentioned in part c and already observed for some 1D gold-thiolate CPs, amorphous [Au(*p*-SPhF)]$_n$ exhibits a phase change from amorphous to crystalline upon heating at 173 °C (see DSC on figure 5a).[12, 19] Thus, the reversible phase change of **2** was studied. The crystalline and red emissive **1** was ground for 30 min in an agate mortar pestle. The compound became non-luminescent and amorphous as shown on the PXRD (figure 6a). This sample was then heated at 150 °C (2 °C.min^{-1}) for 1 minute, and becomes crystalline and luminescent (figure 6a). In a separate experiment, the amorphous phase **2** was heated at the targeted temperature of 150 °C (2 °C.min^{-1}) for 1 minute. After heating, the material became luminescent and its PXRD matched the one of **1** (figure 6b). The SEM images of **1** obtained after phase change is made of aggregates of particles of hundred nanometers corresponding to the particle size of the amorphous phase (figure S22). Then, on grinding the sample for 30 min it became again non-luminescent and amorphous (figure 6b). Hence this gold-thiolate CP displays a cyclic amorphous-crystalline phase change by heating and grinding.

The isothermal crystallization kinetics of [Au(*p*-SPhF)]$_n$ CP

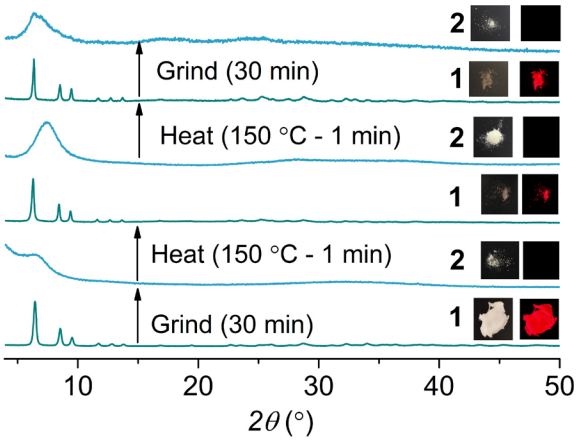

Figure 6. PXRD patterns from down to top of the as-synthesized crystalline phase (**1**) grounded to get the amorphous phase (**2**), which is further heated to return to the crystalline phase (**1**). Then PXRD patterns of as-synthesized amorphous phase (**2**) heated to obtain the crystalline phase (**1**), which is grounded to return to the amorphous phase (**2**). The photos correspond to the samples under natural (left) and UV (right) lights.

was studied by using Avrami equation (eq. 1).

$$X_t = 1 - \exp(-kt^n) \quad \text{.....(1)}$$

Equation 1 (see experimental section in the ESI) gives different kinetic parameters like activation energy (E_a), rate constant (k) and Avrami constant (n, indication crystallization mechanism). Avrami equation is a classic theory to study the solid-solid phase transition.[56-58] This equation and its variants were widely adopted to analyze isothermal and non-isothermal amorphous-crystal phase transition (crystallization) of organic polymers.[59-64] Therefore, this method was utilized to analyze the crystallization process of [Au(*p*-SPhF)]$_n$ to reveal kinetics and mechanism. Based on the DSC experiment carried out under air on figure 5a that shows a T_c at 173 °C, three isotherms at 167 °C, 170 °C

and 173 °C were evaluated by using calorimetry (figure S23). All DSC data were processed and fitted with details shown in the experimental section (ESI). As shown in table S5, the half crystallization time ($t_{1/2}$) decreases with increase of crystallization temperature. At 167 °C, 4.55 min are needed for the [Au(*p*-SPhF)]$_n$ CP to reach 50 % of relative crystallinity. At 170 °C, $t_{1/2}$ decreases to 3.18 min. Further increasing temperature to 173 °C results in a lowest $t_{1/2}$, 2.26 min. The crystallization rate constants (k) at three temperature steps are 1.32×10^{-2} min^{-1} at 167 °C, 3.80×10^{-2} min^{-1} at 170 °C, and 8.30×10^{-2} min^{-1} at 173 °C. Both $t_{1/2}$ and rate constant (k) indicate that crystallization rate has a positive correlation with temperature. Therefore it is expected that the [Au(*p*-SPhF)]$_n$ CP reaches its peak crystallization rate at 173 °C. Furthermore, the Avrami constants (n) are also determined to be 2.7, 2.6, and 2.5, for 167, 170, and 173 °C, respectively, which suggests no dependence of crystallization mechanism on temperature. As no nucleating agent was presented in the sample, [Au(*p*-SPhF)]$_n$ CP crystals grew homogeneously. After knowing both rate constants (k) and Avrami constants (n) at three different temperature steps, the activation energy of crystalizing the [Au(*p*-SPhF)]$_n$ CP was calculated and found to be 164.1 kJ·mol^{-1} (figure S24). Such value is slightly smaller than that of [Au(SPh)]$_n$ CP (197.3 kJ·mol^{-1}).[12] Obtaining these kinetic parameters may help explain the homogeneous growth of [Au(*p*-SPhF)]$_n$ CP crystals. The crystallized [Au(*p*-SPhF)]$_n$ CP exhibited a rod-like morphology as seen in SEM images in accordance with its 1D structure (figure S2). The average Avrami constant of 2.6 suggests a 1D interface-controlled growth mechanism as no nucleating agents are added and there is no change in the chemical composition during the crystallization. This process was maintained through the main crystallization period (from 5 % to 90 % crystallinity) resulting in fibers (rod-like) as observed on the SEM images. Similar values are observed in inorganic phase change chalcogenides.[65-67]

Conclusion

This article shows the versatility of this [Au(*p*-SPhF)]$_n$ CP in term of functionalities and shaping. Indeed, this gold(I)-thiolate CP can be synthesized as amorphous and crystalline phase. The crystalline phase has a 1D double-interpenetrated helices structure that form highly red emissive (QY ~ 70 % at RT) and flexible fibers. Such fibrous luminophore could be inserted into fabrics to fabricate smart luminescent textile.[68] Upon controlled decomposition of this CP by heating between 160 °C to 230 °C, AuNPs can be formed on the surface of the fibers. This bifunctional composite material exhibits both red luminescence and SERS effect and is able to detect BPE molecule. The amorphous phase can form glass with high transparency by heat pressing. Formation of glasses of CPs is a very active field to discover unique properties.[69] Finally, this [Au(*p*-SPhF)]$_n$ CP is also a phase change material, associated to a ON/OFF switch of the emission, and can be a sustainable alternative to the inorganic chalcogenide phase change materials used in the phase change memories.[70-71]

ASSOCIATED CONTENT

The Supporting Information is available free of charge. SEM, TEM, PXRD, crystallographic data, TGA, FTIR, photophysical measurement details and DSC data for the crystalline and amorphous phases, calcined fibers and coordination polymer glass.

AUTHOR INFORMATION

Corresponding Author

*E-mail: aude.demessence@ircelyon.univ-lyon1.fr

ORCID
Shefali Vaidya http://orcid.org/0000-0001-5535-4867
Zeyu Fan https://orcid.org/0009-0004-2431-6285
Tuhin Khan https://orcid.org/0000-0002-2790-3002
Alexandra Fateeva http://orcid.org/0000-0003-3805-6571
François Toche https://orcid.org/0000-0002-8698-114X
Rodica Chiriac http://orcid.org/0000-0003-3149-531X
Gilles Ledoux http://orcid.org/0000-0002-0867-1285
Adel Mesbah https://orcid.org/0000-0002-6905-2402
Satoshi Horike http://orcid.org/0000-0001-8530-6364
Aude Demessence http://orcid.org/0000-0002-8690-5489

Author Contributions

SV: synthesis of crystalline phase, preparation of composite material and their characterizations, steady state spectroscopy (crystalline phase **1**) and initial draft writing of the manuscript; SHa: synthesis of amorphous phase and its characterization, steady state spectroscopy (amorphous phase **2**) and phase change experiments; ZF: fabrication of transparent glass by hot press; TK: steady state spectroscopy (crystalline phase **1**) and pump probe spectroscopy; AF: SEM images; FT and RC: DSC in air; AB: SERS studies; GL: expertise in temperature dependent emission studies; SL, JP, and WJK: simulated FTIR data; JL and XG: crystallization mechanism studies; AM: structural resolution and supervision; SHo: supervision; AD: funding acquisition, supervision and final manuscript writing. The manuscript was written through the contributions of all authors. All authors have given approval to the final version of the manuscript.

Funding Sources

This work was mostly supported by the French National Agency (MEMOL project ANR-16-JTIC-0004-01) and CNRS. Pump probe spectroscopic study was financially supported by the grant GA22-02005S from the Czech Science Foundation (GAČR).

Notes

The authors declare no competing financial interest.

ACKNOWLEDGMENT

SV acknowledges financial support from DKRVO, Czech Republic. The authors acknowledge SOLEIL synchrotron (Gif-sur-Yvette, France) for provision radiation facilities (BAG for X-ray diffraction 20201440) and Erik Elkaïm for assistance in using CRISTAL beamline, the Centre Technologique des Microstructures of the University of Lyon for providing the electron microscopy facilities. AD is grateful to the CNRS for her EMERGENCE support. SHa acknowledges the CNRS for her PhD grant and JSPS for her travel funding to Japan. WJK and SL acknowledge financial support from the French-Korean program STAR. All authors thank Dr. Buqin Xu and Alexis Giraudon for their help in the revision process.

ABBREVIATIONS

CPs, coordination polymers; PXRD, powder X-ray diffraction; PDF, pair distribution function; TGA, thermogravimetric analysis; SEM, scanning electron microscopy; TEM, transmission electron microscopy; FTIR, Fourier transform infrared; DFT, density functional theory; RT, room temperature; QY, quantum yield; ESA, excited state absorption; LMCT, ligand to metal charge transfer; LC, ligand centered; TA, transient absorption; AuNPs, gold nano-particles; SERS, Surface-enhanced Raman spectroscopy; BPE, 1,2-bis(4-pyridyl)ethylene; T_g, glass transition temperature; DSC, differential scanning calorimetry.

REFERENCES

1. Battocchio, C.; Porcaro, F.; Mukherjee, S.; Magnano, E.; Nappini, S.; Fratoddi, I.; Quintiliani, M.; Russo, M. V.; Polzonetti, G., Gold Nanoparticles Stabilized with Aromatic Thiols: Interaction at the Molecule–Metal Interface and Ligand Arrangement in the Molecular Shell Investigated by SR-XPS and NEXAFS. *J. Phys . Chem. C* **2014,** *118* (15), 8159.
2. Xue, Y.; Li, X.; Li, H.; Zhang, W., Quantifying thiol–gold interactions towards the efficient strength control. *Nat. Commun .* **2014,** *5* (1), 4348.
3. Vericat, C.; Vela, M. E.; Benitez, G.; Carro, P.; Salvarezza, R. C., Self-assembled monolayers of thiols and dithiols on gold: new challenges for a well-known system. *Chem. Soc. Rev.* **2010,** *39* (5), 1805.
4. Candreva, A.; Di Maio, G.; Parisi, F.; Scarpelli, F.; Crispini, A.; Godbert, N.; Ricciardi, L.; Nucera, A.; Rizzuto, C.; Barberi, R. C.; Castriota, M.; La Deda, M. Luminescent Self-Assembled Monolayer on Gold Nanoparticles: Tuning of Emission According to the Surface Curvature *Chemosensors*, **2022**, *10(5)*, 176.
5. Yeh, Y.-C.; Creran, B.; Rotello, V. M., Gold nanoparticles: preparation, properties, and applications in bionanotechnology. *Nanoscale* **2012,** *4* (6), 1871.
6. Ghosh, P.; Han, G.; De, M.; Kim, C. K.; Rotello, V. M., Gold nanoparticles in delivery applications. *Adv. Drug Deliv. Rev.* **2008,** *60* (11), 1307.
7. Llevot, A.; Astruc, D., Applications of vectorized gold nanoparticles to the diagnosis and therapy of cancer. *Chem. Soc. Rev.* **2012,** *41* (1), 242.
8. Wang, W.; Wei, Q.-Q.; Wang, J.; Wang, B.-C.; Zhang, S.-h.; Yuan, Z., Role of thiol-containing polyethylene glycol (thiol-PEG) in the modification process of gold nanoparticles (AuNPs): Stabilizer or coagulant? *J. Colloid Interface Sci.* **2013,** *404*, 223.
9. Yan, C.; Yuan, R.; Pfalzgraff, W. C.; Nishida, J.; Wang, L.; Markland, T. E.; Fayer, M. D., Unraveling the dynamics and structure of functionalized self-assembled monolayers on gold using 2D IR spectroscopy and MD simulations. *Proc. Natl. Acad. Sci. U.S.A.* **2016,** *113* (18), 4929.
10. Yu, C.; Zhu, L.; Zhang, R.; Wang, X.; Guo, C.; Sun, P.; Xue, G., Investigation on the Mechanism of the Synthesis of Gold(I) Thiolate Complexes by NMR. *J. Phys . Chem. C* **2014,** *118* (19), 10434.
11. Al-Sa'ady, A. K. H.; Moss, K.; McAuliffe, C. A.; Parish, R. V., Mössbauer and nuclear magnetic resonance spectroscopic studies on 'Myocrisin', 'Solganol', 'Auranofin', and related gold(I) thiolates. *J. Chem. Soc., Dalton Trans.* **1984,** (8), 1609.
12. Lavenn, C.; Okhrimenko, L.; Guillou, N.; Monge, M.; Ledoux, G.; Dujardin, C.; Chiriac, R.; Fateeva, A.; Demessence, A., A luminescent double helical gold(i)–thiophenolate coordination polymer obtained by hydrothermal synthesis or by thermal solid-state amorphous-to-crystalline isomerization. *J. Mater. Chem. C* **2015,** *3* (16), 4115.
13. Söptei, B.; Mihály, J.; Szigyártó, I. C.; Wacha, A.; Németh, C.; Bertóti, I.; May, Z.; Baranyai, P.; Sajó, I. E.; Bóta, A., The supramolecular chemistry of gold and l-cysteine: Formation of photoluminescent, orange-emitting assemblies with multilayer structure. *Colloids Surf. A: Physicochem. Eng. Asp.* **2015,** *470*, 8.
14. Leff, D. V.; Ohara, P. C.; Heath, J. R.; Gelbart, W. M., Thermodynamic Control of Gold Nanocrystal Size: Experiment and Theory. *J. Phys . Chem.* **1995,** *99* (18), 7036.
15. Brust, M.; Walker, M.; Bethell, D.; Schiffrin, D. J.; Whyman, R., Synthesis of thiol-derivatised gold nanoparticles in a two-phase Liquid–Liquid system. *J. Chem. Soc., Chem. Commun.* **1994,** (7), 801.
16. Shimmin, R. G.; Schoch, A. B.; Braun, P. V., Polymer Size and Concentration Effects on the Size of Gold Nanoparticles Capped by Polymeric Thiols. *Langmuir* **2004,** *20* (13), 5613.
17. Veselska, O.; Demessence, A., d10 coinage metal organic chalcogenolates: From oligomers to coordination polymers. *Coord. Chem. Rev.* **2018,** *355*, 240.
18. Nie, H.; Li, M.; Hao, Y.; Wang, X.; Gao, S.; Wang, P.; Ju, B.; Zhang, S. X.-A., Morphology modulation and application of Au(i)–thiolate nanostructures. *RSC Adv.* **2014,** *4* (92), 50521.
19. Veselska, O.; Vaidya, S.; Das, C.; Guillou, N.; Bordet, P.; Fateeva, A.; Toche, F.; Chiriac, R.; Ledoux, G.; Wuttke, S.; Horike, S.; Demessence, A., Cyclic Solid-State Multiple Phase Changes with Tuned Photoemission in a Gold Thiolate Coordination Polymer. *Angew. Chem. Int. Ed .* **2022,** *61* (14), e202117261.
20. Rawashdeh-Omary, M. A.; Omary, M. A.; Patterson, H. H.; Fackler, J. P., Excited-State Interactions for [Au(CN)2-]n and [Ag(CN)2-]n Oligomers in Solution. Formation of Luminescent Gold−Gold Bonded Excimers and Exciplexes. *J. Am. Chem. Soc.* **2001,** *123* (45), 11237.
21. Roberts, R. J.; Le, D.; Leznoff, D. B., Controlling intermolecular aurophilicity in emissive dinuclear Au(i) materials and their luminescent response to ammonia vapour. *Chem. Commun.* **2015,** *51* (76), 14299.
22. Veselska, O.; Okhrimenko, L.; Guillou, N.; Podbevšek, D.; Ledoux, G.; Dujardin, C.; Monge, M.; Chevrier, D. M.; Yang, R.; Zhang, P.; Fateeva, A.; Demessence, A., An intrinsic dual-emitting gold thiolate coordination polymer, [Au(+I)(p-SPhCO2H)]n, for ratiometric temperature sensing. *Journal of Materials Chemistry C* **2017,** *5* (38), 9843.
23. Vaidya, S.; Veselska, O.; Zhadan, A.; Daniel, M.; Ledoux, G.; Fateeva, A.; Tsuruoka, T.; Demessence, A., Flexible and luminescent fibers of a 1D Au(i)–thiophenolate coordination polymer and formation of gold nanoparticle-based composite materials for SERS. *J. Mater. Chem. C* **2020,** *8* (24), 8018.
24. Al-Mahamad, L. L. G.; El-Zubir, O.; Smith, D. G.; Horrocks, B. R.; Houlton, A., A coordination polymer for the site-specific integration of semiconducting sequences into DNA-based materials. *Nat. Commun.* **2017,** *8*, 720.
25. Vaidya, S.; Veselska, O.; Zhadan, A.; Diaz-Lopez, M.; Joly, Y.; Bordet, P.; Guillou, N.; Dujardin, C.; Ledoux, G.; Toche, F.; Chiriac, R.; Fateeva, A.; Horike, S.; Demessence, A., Transparent and luminescent glasses of gold thiolate coordination polymers. *Chem. Sci.* **2020,** *11* (26), 6815.
26. Wuttig, M.; Yamada, N., Phase-change materials for rewriteable data storage. *Nat. Mater.* **2007,** *6* (11), 824.
27. Veselska, O.; Guillou, N.; Diaz-Lopez, M.; Bordet, P.; Ledoux, G.; Lebègue, S.; Mesbah, A.; Fateeva, A.; Demessence, A., Sustainable and Efficient Low-Energy Light Emitters: A Series of One-Dimensional d10 Coinage Metal–Organic

Chalcogenolates, [M(o-SPhCO2H)]n. *ChemPhotoChem* **2022,** *6* (5), e202200030.
28. Abdallah, A.; Vaidya, S.; Hawila, S.; Ornis, S.-L.; Nebois, G.; Barnet, A.; Guillou, N.; Fateeva, A.; Mesbah, A.; Ledoux, G.; Bérut, A.; Vanel, L.; Demessence, A., Luminescent and sustainable d10 coinage metal thiolate coordination polymers for high-temperature optical sensing. *iScience* **2023,** *26* (2), 106016.
29. Pyykkö, P., Strong Closed-Shell Interactions in Inorganic Chemistry. *Chem. Rev.* **1997,** *97* (3), 597.
30. Sculfort, S.; Braunstein, P., Intramolecular d10–d10 interactions in heterometallic clusters of the transition metals. *Chem. Soc. Rev.* **2011,** *40* (5), 2741.
31. Schmidbaur, H.; Schier, A., Aurophilic interactions as a subject of current research: an up-date. *Chem. Soc. Rev.* **2012,** *41* (1), 370.
32. Thalladi, V. R.; Weiss, H.-C.; Bläser, D.; Boese, R.; Nangia, A.; Desiraju, G. R., C–H···F Interactions in the Crystal Structures of Some Fluorobenzenes. *J. Am. Chem. Soc.* **1998,** *120* (34), 8702.
33. Hawila, S.; Massuyeau, F.; Gautier, R.; Fateeva, A.; Lebègue, S.; Kim, W. J.; Ledoux, G.; Mesbah, A.; Demessence, A., Tuning the 1D–2D dimensionality upon ligand exchange in silver thiolate coordination polymers with photoemission switching. *J. Mater. Chem. B* **2023,** *11* (18), 3979.
34. Assefa, Z.; McBurnett, B. G.; Staples, R. J.; Fackler, J. P.; Assmann, B.; Angermaier, K.; Schmidbaur, H., Syntheses, Structures, and Spectroscopic Properties of Gold(I) Complexes of 1,3,5-Triaza-7-phosphaadamantane (TPA). Correlation of the Supramolecular Au.cntdot. .cntdot. .cntdot.Au Interaction and Photoluminescence for the Species (TPA)AuCl and [(TPA-HCl)AuCl]. *Inorg. Chem.* **1995,** *34* (1), 75.
35. Milián Medina, B.; Beljonne, D.; Egelhaaf, H.-J.; Gierschner, J., Effect of fluorination on the electronic structure and optical excitations of π-conjugated molecules. *J. Chem. Phys.* **2007,** *126* (11), 111101.
36. Dedeian, K.; Shi, J.; Shepherd, N.; Forsythe, E.; Morton, D. C., Photophysical and Electrochemical Properties of Heteroleptic Tris-Cyclometalated Iridium(III) Complexes. *Inorg. Chem.* **2005,** *44* (13), 4445.
37. Lemes, M. A.; do Nascimento Neto, J. A.; Fernandes Guimarães, F.; Maia, L. J. Q.; de Santana, R. C.; Terra Martins, F., Secondary ligands and the intramolecular hydrogen bonds drive photoluminescence quantum yields from aminopyrazine coordination polymers. *New J. Chem.* **2020,** *44* (46), 20259.
38. Thomas, J. C.; Goronzy, D. P.; Dragomiretskiy, K.; Zosso, D.; Gilles, J.; Osher, S. J.; Bertozzi, A. L.; Weiss, P. S., Mapping Buried Hydrogen-Bonding Networks. *ACS Nano* **2016,** *10* (5), 5446.
39. Forward, J. M.; Bohmann, D.; Fackler, J. P., Jr.; Staples, R. J., Luminescence Studies of Gold(I) Thiolate Complexes. *Inorg. Chem.* **1995,** *34* (25), 6330.
40. Chergui, M., Ultrafast Photophysics of Transition Metal Complexes. Acc. Chem. Res. **2015,** *48* (3), 801.
41. Aguiló, E.; Moro, A. J.; Outis, M.; Pina, J.; Sarmento, D.; Seixas de Melo, J. S.; Rodríguez, L.; Lima, J. C., Deactivation Routes in Gold(I) Polypyridyl Complexes: Internal Conversion Vs Fast Intersystem Crossing. *Inorg. Chem.* **2018,** *57* (21), 13423.
42. Vogt, R. A.; Gray, T. G.; Crespo-Hernández, C. E., Subpicosecond Intersystem Crossing in Mono- and Di(organophosphine)gold(I) Naphthalene Derivatives in Solution. *J. Am. Chem. Soc.* **2012,** *134* (36), 14808.
43. Hamze, R.; Shi, S.; Kapper, S. C.; Muthiah Ravinson, D. S.; Estergreen, L.; Jung, M.-C.; Tadle, A. C.; Haiges, R.; Djurovich, P. I.; Peltier, J. L.; Jazzar, R.; Bertrand, G.; Bradforth, S. E.; Thompson, M. E., "Quick-Silver" from a Systematic Study of Highly Luminescent, Two-Coordinate, d10 Coinage Metal Complexes. J. Am. Chem. Soc. **2019,** *141* (21), 8616.
44. Ashfold, M. N. R.; Devine, A. L.; Dixon, R. N.; King, G. A.; Nix, M. G. D.; Oliver, T. A. A., Exploring nuclear motion through conical intersections in the UV photodissociation of phenols and thiophenol. *Proc. Natl. Acad. Sci. U.S.A.* **2008,** *105* (35), 12701.
45. Pluchery, O.; Bryche, J.-F., *An Introduction to Plasmonics*. World Scientific: 2023.
46. Scaiano, J. C.; Stamplecoskie, K. G.; Hallett-Tapley, G. L., Photochemical Norrish type I reaction as a tool for metal nanoparticle synthesis: importance of proton coupled electron transfer. *Chem. Commun.* **2012,** *48* (40), 4798.
47. Fujiwara, K.; Akutsu, T.; Gonome, H., Enhancing Plasmon Excitation of Small Au Nanoparticles via Light Scattering from Metal-Oxide Supports. *J. Phys . Chem. C* **2022,** *126* (22), 9509.
48. He, M.; Zhang, N.-T.; Yu, X.-Y.; Jia, Y.; Sun, B.; Meng, F.-L.; Jin, Z.; Liu, J.-H.; Luo, T., Synthesis of Porous Gold Based on Gold–Thiol Coordination Polymer and Its Application in SERS Detection with High Activity and High Reproducibility. *Chem. Lett.* **2013,** *42* (4), 407.
49. Wang, Y.; Polavarapu, L.; Liz-Marzán, L. M., Reduced Graphene Oxide-Supported Gold Nanostars for Improved SERS Sensing and Drug Delivery. *ACS Appl. Mater. Interfaces.* **2014,** *6* (24), 21798.
50. Merga, G.; Saucedo, N.; Cass, L. C.; Puthussery, J.; Meisel, D., "Naked" Gold Nanoparticles: Synthesis, Characterization, Catalytic Hydrogen Evolution, and SERS. *J. Phys . Chem. C* **2010,** *114* (35), 14811.
51. Herrera, G. M.; Padilla, A. C.; Hernandez-Rivera, S. P., Surface Enhanced Raman Scattering (SERS) Studies of Gold and Silver Nanoparticles Prepared by Laser Ablation. *Nanomaterials* **2013,** *3* (1), 158.
52. Michota, A.; Bukowska, J., Surface-enhanced Raman scattering (SERS) of 4-mercaptobenzoic acid on silver and gold substrates. *J. Raman Spectrosc.* **2003,** *34* (1), 21.
53. Saini, A.; Medwal, R.; Bedi, S.; Mehta, B.; Gupta, R.; Maurer, T.; Plain, J.; Annapoorni, S., Axonic Au Tips Induced Enhancement in Raman Spectra and Biomolecular Sensing. *Plasmonics* **2015,** *10* (3), 617.
54. Herrera, G. M.; Padilla, A. C.; Hernandez-Rivera, S. P. Surface Enhanced Raman Scattering (SERS) Studies of Gold and Silver Nanoparticles Prepared by Laser Ablation *Nanomaterials*, **2013**, *3(1)*, 158.
55. Félidj, N.; Aubard, J.; Lévi, G.; Krenn, J. R.; Hohenau, A.; Schider, G.; Leitner, A.; Aussenegg, F. R., Optimized surface-enhanced Raman scattering on gold nanoparticle arrays. *Appl. Phys. Lett.* **2003,** *82* (18), 3095.
56. Avrami, M., Kinetics of Phase Change. II Transformation-Time Relations for Random Distribution of Nuclei. *J. Chem. Phys.* **1940,** *8* (2), 212.
57. Avrami, M., Kinetics of Phase Change. I General Theory. *J. Chem. Phys.* **1939,** *7* (12), 1103.
58. Avrami, M., Granulation, Phase Change, and Microstructure Kinetics of Phase Change. III. *J. Chem. Phys.* **1941,** *9* (2), 177.
59. Cai, J.; Liu, M.; Wang, L.; Yao, K.; Li, S.; Xiong, H., Isothermal crystallization kinetics of thermoplastic starch/poly(lactic acid) composites. *Carbohydr. Polym.* **2011,** *86* (2), 941.
60. Pantani, R.; De Santis, F.; Sorrentino, A.; De Maio, F.; Titomanlio, G., Crystallization kinetics of virgin and processed poly(lactic acid). *Polym. Degrad. Stab.* **2010,** *95* (7), 1148.

61. Nofar, M.; Zhu, W.; Park, C. B.; Randall, J., Crystallization Kinetics of Linear and Long-Chain-Branched Polylactide. *Ind. Eng. Chem. Res.* **2011,** *50* (24), 13789.
62. Sencadas, V.; Martins, P.; Pitães, A.; Benelmekki, M.; Gómez Ribelles, J. L.; Lanceros-Mendez, S., Influence of Ferrite Nanoparticle Type and Content on the Crystallization Kinetics and Electroactive Phase Nucleation of Poly(vinylidene fluoride). *Langmuir* **2011,** *27* (11), 7241.
63. Jimenez, A. M.; Krauskopf, A. A.; Pérez-Camargo, R. A.; Zhao, D.; Pribyl, J.; Jestin, J.; Benicewicz, B. C.; Müller, A. J.; Kumar, S. K., Effects of Hairy Nanoparticles on Polymer Crystallization Kinetics. *Macromolecules* **2019,** *52* (23), 9186.
64. Castillo, R. V.; Müller, A. J.; Raquez, J.-M.; Dubois, P., Crystallization Kinetics and Morphology of Biodegradable Double Crystalline PLLA-b-PCL Diblock Copolymers. *Macromolecules* **2010,** *43* (9), 4149.
65. Friedrich, D.; Schlosser, M.; Weihrich, R.; Pfitzner, A., Polymorphism of CsGaS2 – structural characterization of a new two-dimensional polymorph and study of the phase-transition kinetics. *Inorg. Chem. Front.* **2017,** *4* (2), 393.
66. Lafi, O. A., Glass transition kinetics and crystallization mechanism in Se90Cd8Bi2 and Se90Cd6Bi4 chalcogenide glasses. *J. Alloys Compd.* **2012,** *519*, 123.
67. Li, L.; Yin, H.; Wang, Y.; Zheng, J.; Zeng, H.; Chen, G., Study on crystallization behavior of novel silver chloride based chalcogenide glasses. *J. Alloys Compd.* **2017,** *706*, 48.
68. Jia, L.-W.; Zhang, X., Versatile Red-Emissive Carbon Dots for Smart Textiles and Fluorescence Sensing. *ACS Appl. Nano Mater.* **2023,** *6* (2), 1379.
69. Wei, Y.-S.; Ashling, C. W.; Watcharatpong, T.; Fan, Z.; Horike, S., Hierarchical Metal-Organic Network-Forming Glasses toward Applications. *Adv. Funct. Mater.* **2023**, 2307226.
70. Guo, P.; Sarangan, A. M.; Agha, I., A Review of Germanium-Antimony-Telluride Phase Change Materials for Non-Volatile Memories and Optical Modulators. *Appl. Sci.* **2019,** *9* (3), 530.
71. Wuttig, M.; Raoux, S., The Science and Technology of Phase Change Materials. *Z. Anorg. Allg. Chem.* **2012,** *638*, 2455.

TOC